Periodica Polytechnica
Mechanical Engineering

On the Stress Distribution in Slotted Cylinder Springs

62(2), pp. 136-147, 2018
https://doi.org/10.3311/PPme.11392

Gérard Mbobda[1], Lucien Meva'a[1],
Pascal Luprince Kouokam Mbobda[2]

RESEARCH ARTICLE

Received 17 August 2017; accepted after revision 06 January 2017

Abstract

A critical analysis of the scientific literature shows that, contrary to helical and other springs widely used in practice, slotted cylinder springs have been insufficiently documented to date. Currently, given the under exploited potential of their particular mechanical properties, a further investigation is much necessary in order to extend their use to as many as possible areas of technology. This is quite possible thanks to the most recent state of mechanical design research and technology. This paper is a part of a project that aims at developing specific computer software tools allowing precise analytic stress state determination. It develops a statically indeterminate approach of the problem of the stress behaviour of such springs, following which previously and three newly proposed models are compared one with another on the basis of ratios between Von Mises' stresses. Finally, for the case of two slots per section slotted cylinder springs, it is concluded that the analytical solution of the two degrees of freedom proposed primary system is in good agreement with empirical and Computer Aid Design res-olutions. A generalization to higher number of slots per section springs is foreseen using the same methodology.

Keywords

slotted cylinder springs, structural modelling, Von Mises' stresses computer simulation

[1] Department of Industrial and Mechanical Engineering,
National Advanced School of Engineering, Yaoundé, P.O.B. 8390, Cameroon

[2] Department of Physics, Faculty of science, University of Yaoundé,
P.O.B. 837, Cameroon

* Corresponding author, e-mail: gmbobda@gmail.com

1 Introduction

Slotted cylinder springs are obtained by machining open slots on cylindrical rings. They operate like a set of flat coaxial elastic circular beams put in series and linked to one another by supports (Fig. 1). They are used where excellent dynamic and vibration qualities are needed.

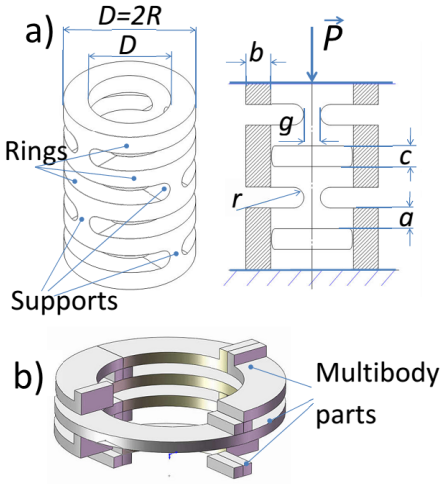

Fig. 1 Slotted cylinder spring: a) Design parameters, b) CAD Multibody modelling

They can secure against propagation of vibrations between mechanical systems joined parts. They are capable of absorbing loads to such a range which is impossible in the case of conventional helical springs [1, 2]. Used as shock-absorbers or vibration isolator [3], they are excellent dissipators and accumulators of energy. They are also used as transducers for the generation of seismic waves in electromechanical equipment, bridges and buildings and to damp earthquakes.

Among the many types and forms of springs, slotted springs are unique [4] for the reason that they can be used in reduced space constructions needing high stiffness elastic elements and can be extremely small in size for a very wide range of stiffness whose upper bound exceeds by far all stiffness values which can reasonably be achieved with conventional elastic elements and which come close to that of the solid material. One of

their most important advantages over the helical springs coiled from round cross-section wire is that the execution of the latter is possible only when their minimal diameter is much bigger than the wire diameter. Another advantage of constructions made with them is simplicity in fastening because their mounting can be designed in such a way that some of parts form one unit with the springs and work together in the stretching and compression processes.

Moreover, contrary to springs coiled from wire, their material does not suffer from the lack of self-stresses and their mechanical characteristics are of high accuracy. So, they are to be recommended for use in systems, where compactness, great stiffness and high accuracy of positioning are necessary. Consequently, their performance and successful implementation requires a good choice of geometrical parameters, maximum load and deformation and structural stability.

Nevertheless, very few research papers and books can be found on the study of their behaviour against static and dynamic loadings. Generally, the laws governing the static behavior of a curved beam are defined by equilibrium equations. Their interpretation by means of energy equations allows to reach good results not only for circular, parabolic and elliptical beams structures loaded in plane [7-12], but also for circular beams loaded perpendicularly to their planes [13, 14, 15]. However, the nature of the ring-support links of the slotted cylinder springs makes more complex their behavior in comparison with that of the curved beams. Besides, on the fringes of finite element studies[6, 16, 17], till today, little has been done concerning such structures as three-dimensional, non-planar, or coupled lateral-torsional statically indeterminate systems.

2 Experimental and modelling backgrounds

The first scientific published technical information about slotted cylinder springs dates from 1963 by Winhelm A. Schneider [4] who on the basis of experimental data presented an approach to design and application. He emphasized their use as elastic elements of controllable compliance in seismic transducers and established that their performance can be compared with that of conventional springs. According to him, this type of spring offers unique characteristics of high load capacity and low deflection in extremely small size.

Rivin E. put forward [5] in the year 2003, approximate empirical formula for the calculation of the slotted cylinder spring characteristics:

$$\sigma_{ef} = \frac{k_g P D_N}{\beta a b^2} \tag{1}$$

where *a, b* are the height and the thickness of the ring section; *D, D_N*– the spring external and nominal diameter; *P*- the force loading the spring, *i* – the number of active rings, [σ] – the admissible normal stress; β and α_n, coefficients as a function of the ratio *b/a*.

Krzysztof Michalczyk [6] made an attempt to verify (1) by FEM modelling from structural elements SOLID92 in the environment of ANSYS software. The configurations that he proposed are that with two perpendicular planes of symmetry, crossing each other at spring axis. This means that supports are not bent to sides as a result of pressing the spring. Therefore according to that author, just only a quarter of the ring with supports propping it up can be modeled as fixed on its edges beam with supports shifted in parallel with each other (Fig.2a). He assumes that angular deflections of rings are small and concludes that in the middle of such a beam (point C) the value of bending moment is equal to zero. By cutting this beam in the middle, one achieves two beams with one end fixed and the second one free. Then, in order to keep the same values of moments in these cut beams as in the one not cut, the free ends of beams (Fig. 2b) receive. vertical forces in value of quarter of entire load.

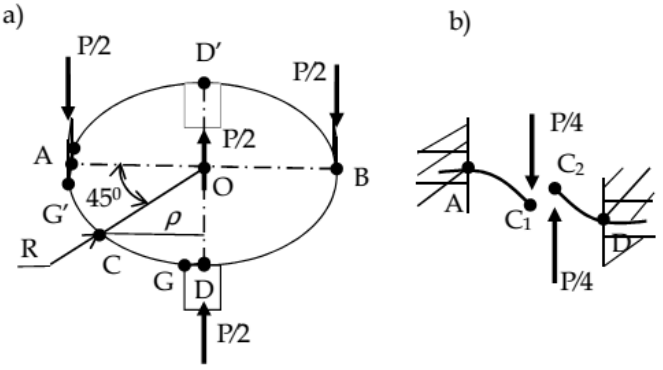

Fig. 2 Krzysztof Michalczyk's modelling of the slotted spring ring [6]

As a result, the bending stress σ_{Gp} and the shear stress τ_1 in the ring are:

$$\sigma_{Gp} = \frac{M_g}{W_x} = \frac{3P\left(\rho - \frac{g}{2}\right)}{2ba^2} \tag{2}$$

$$\tau_1 = \frac{P}{4ab} \tag{3}$$

The torsional stress in a rectangular cross section bar is given by Saint-Venant's formula:

$$\tau_{Ms} = \frac{M_s}{\mu a b^2} = \frac{P}{4}\rho \tag{4}$$

where $M_s = \frac{P}{4}\rho$ and $\mu = \frac{a}{3a + 1.8b}$;

Referring to Von Mises formula, the value of substitutional stresses is calculated as:

$$\sigma_{HMH} = \left[\sigma_{Gp}{}^2 + 3\left(\tau_T + \tau_{Ms}\right)^2\right]^{1/2} \tag{5}$$

Since in real conditions configuration is not flat but spatial, the stresses appearing in a considered ring beam will have a

complex nature. In this formula, in order to take into account stress concentration depending on geometry, two empirical coefficients are introduced. Finally, the formula to calculate maximum stresses in slotted spring takes the form:

$$\sigma_{E\max} = \alpha\ \delta\ \sigma_{HMH} \tag{6}$$

where:

α, stress concentration coefficient: $\alpha = 1$ for $a/c = 1$ and $\alpha = 1.3$ for $a/c = 1.5$

δ, inequality of stress distribution coefficient:

$$\delta = 1 + \left(\frac{b}{D}\right)^{1/2}$$

The corresponding method of calculating stresses in slotted cylinder springs is more time-consuming, compared to the earlier, but is worth for its high accuracy relatively to the preceding ones.

3 Using force method to stress analysis of slotted cylinder springs

3.1 Some CAD simulation conclusions

3.1.1 Modelling springs with fillet radius r=0

A special test bench using lathe equipment was designed and created for the verification of diverse theoretical assumptions on the slotted cylinder springs. Its principle consists of the comparison of the deflections of the slotted cylinder loaded together with a basic helical spring mounted on the lathe axis. The external loads are measured by means of comparators with 1 micron precision.

In parallel, we carried a study based on:

- multi-body part model design (Fig. 1b, Fig. 3b,e)
- hiding and suppressing part components from the created multi-body models
- static simulation of multi-models comprising hidden or suppressed parts.

Accordingly, two slots per section, two rings steel slotted cylinder springs were created (Fig. 3a) with a main dimensions range including that recommended [6]: $D = 20 - 50$mm, $a = 3 - 5$mm, $b = 1 - 9$mm, $c = 2 - 3$mm, $g = 3 - 5$mm, $r \approx 0$mm.

From the static simulation, the following interesting facts were observed:

a) The ring plane section at point C has no rotation relatively to the ring neutral (or tangential axis).

b) The upper ring horizontal at point D for the supports directly submitted to external vertical load (Fig. 3a-b) turns significantly relatively to the ring neutral axis. The horizontal plane of the intermediate ring at point D for the spring whose upper ring is directly submitted to the external vertical load (Fig. 3c-f) has a very small angular deflection relatively to the neutral axis.

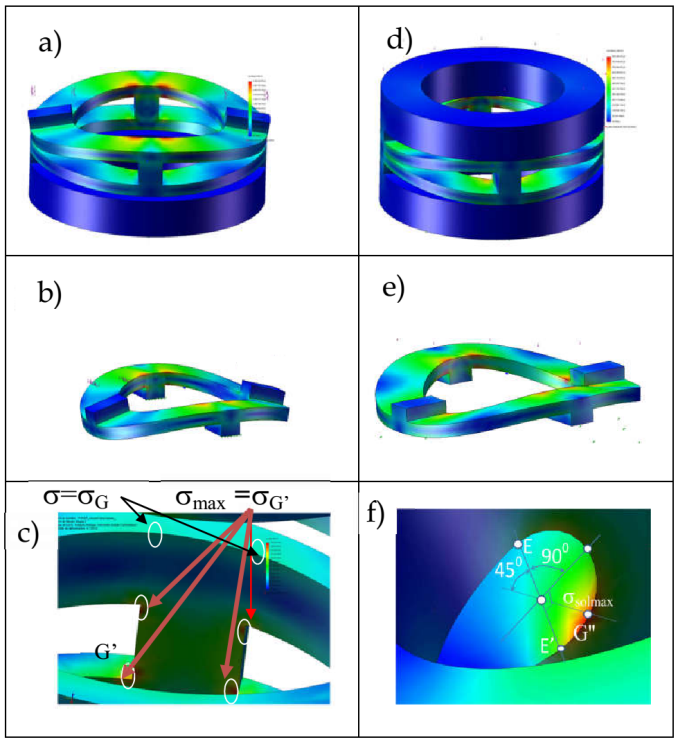

Fig. 3 deflection and stress of springs: a-b) loaded from ring supports; d-e) loaded from the upper ring; c-f), stress state around points G and G'

3.1.2 CAD simulation major drawbacks

In reality, the form of the slotted cylinder spring presents potentially sources of singularities due to high stress concentration near the 90 degree corners between the supports and the rings and at the sharp inner internal edges. On this topic, in order to increase the reliability of the meshing in solidworks, the quality chosen was "fine" and the density parameter "standard". The difference between the results obtained for the mid and the "fine" positions was calculated. Its value is less than 5% for a mesh size varying from 1.5-0.08 to 0.03-0.65. Moreover, in practice, it is unacceptable to manufacture springs with $r = 0$. Chamfer and fillet are introduced by means of the cutting tool shape or other method. Radius $r = c$ is easily obtained as drawn in Fig. 1.

3.2 Slotted cylinder springs as one d.o.f indeterminate systems (first model)

A way of solving the problem of displacement in slotted cylinder springs is to consider a spring ring as a spatial, statically indeterminate structure of one degree of freedom made of a curved beam. Just as above, let's study a quarter of a ring (Fig. 3a). Assuming that the section C (R, $\pi/4$) situated 45^0 from the clamped end section does not rotate relatively to D(R,0), but just moves in the axial direction we conclude that in the normal section passing through C appear a shearing force $\boldsymbol{F}_s = \boldsymbol{Q}$ and an unknown torsional moment $\boldsymbol{X}_1$. Subsequently, the original system is replaced by a primary system made of the part of the spring ring going from A to C under external loads $\boldsymbol{Q}$ and $\boldsymbol{X}_1$ (Fig. 4b,c). Note that in this case, C is the $\boldsymbol{X}_1$ application point.

In the following, let's denote by:

X, ***Y***, unknown internal torsional and bending torques in springs, indexes *N* and *T,* the radial (bending) and tangential (torsional) components,

δ_{ij}, displacement at $\boldsymbol{X}_i$ application point at $\boldsymbol{X}_i$ direction from $X_j = 1$ only, in the primary system,

δ_{iQ}, displacement at $\boldsymbol{X}_i$ application point at $\boldsymbol{X}_i$ direction from external load only, the primary system,

Δ_i, displacement at $\boldsymbol{X}_i$ application point at $\boldsymbol{X}_i$ direction from all loads - external load and all unknown values, $\boldsymbol{M}_{QN}$ and $\boldsymbol{M}_{QT}$, the bending and the torsional moments due to the force $\boldsymbol{Q}$ only, at the application point,

$\boldsymbol{M}_{Q}$, the total moment due to the force $\boldsymbol{Q}$ only, applied at the application point, in the primary system.

$\boldsymbol{M}_{Xi}$, $\boldsymbol{M}_{Xi}$, the internal moment due to the torque $\boldsymbol{X}_i$,

γ the half of the angle corresponding to the support width (Fig. 4d).

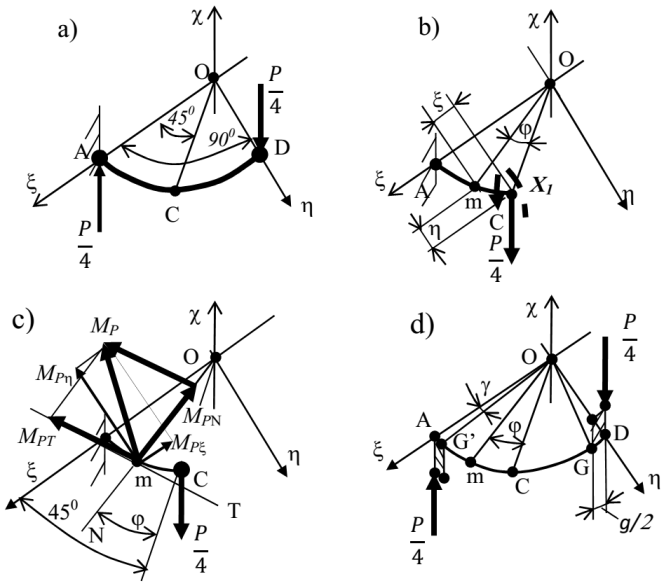

Fig. 4 Reduction of the internal load to a superposition of the force $Q = P/4$ and the torque $X_1(M_N, M_T)$ acting at point C.

The elastic strain energy stored in the quarter of beam along the ring neutral axis l_λ is determined as:

$$\begin{aligned} U &= U_N + M_T \\ &= \frac{1}{2EI}\int_{l_\lambda} M_{XiN}{}^2 ds + \frac{1}{2GI_P}\int_{l_\lambda} M_{XiT}{}^2 ds \\ &= \frac{1}{2EI}\int_0^{\frac{\pi}{2}} M_{XiN}{}^2 R d\varphi + \frac{1}{2GI_P}\int_0^{\frac{\pi}{2}} M_{XiT}{}^2 R d\varphi \end{aligned}$$

From the Castigliano's theorem:

$$\delta_{ij} = \Sigma\frac{\partial Ui}{\partial Xj} = \frac{1}{EI}\int_0^{\frac{\pi}{2}} M_{XiN}(\varphi)\frac{\partial M_{XiN}}{\partial XiN} R d\varphi + \frac{1}{2GI_P}\int_0^{\frac{\pi}{2}} M_{XiT}(\varphi)\frac{\partial M_{XiT}}{\partial XiT} R d\varphi$$

Therefore:

$$\delta_{ij}\ X_i + \delta_{iQ} = \Delta_i = 0 \tag{7}$$

From Fig. 4c we have:

$$\begin{cases} M_{Q\xi} = \dfrac{PR}{4}\sin\dfrac{\pi}{4} - \dfrac{PR}{4}\sin\left(\dfrac{\pi}{4}-\varphi\right) \\ M_{Q\eta} = \dfrac{PR}{4}\cos\dfrac{\pi}{4} + \dfrac{PR}{4}\cos\left(\dfrac{\pi}{4}-\varphi\right) \end{cases}$$

Then

$$\begin{cases} M_{QN} = M_{Q\xi}\cos\left(\dfrac{\pi}{4}-\varphi\right) + M_{Q\eta}\sin\left(\dfrac{\pi}{4}-\varphi\right) \\ M_{QT} = M_{Q\xi}\sin\left(\dfrac{\pi}{4}-\varphi\right) + M_{Q\eta}\cos\left(\dfrac{\pi}{4}-\varphi\right) \end{cases}$$

Finally,

$$\begin{cases} M_{QN} = -\dfrac{PR}{4}\sin\varphi \\ M_{QT} = -\dfrac{PR}{4}(1-\cos\varphi) \\ M_Q = M_{QN}{}^2 + M_{QT}{}^2 \end{cases} \tag{8}$$

$$\begin{cases} \dfrac{\partial X_{1N}}{\partial X1} = \dfrac{\partial X_1\sin\varphi}{\partial X1} = \sin\varphi \\ \dfrac{\partial X_{1T}}{\partial X1} = \dfrac{\partial X_1\cos\varphi}{\partial X1} = \cos\varphi \end{cases} \tag{9}$$

The total bending and torsional moments at point m(R,φ) are:

$$\begin{cases} M_{mN} = X_1\sin\varphi - \dfrac{PR}{4}\sin\varphi \\ M_{mT} = X_1\cos\varphi + \dfrac{PR}{4}(1-\cos\varphi) \end{cases} \tag{10}$$

Let g be the support width (Fig. 4d) and γ the angle between OG and Oη (or between OG' and Oξ). Then, the total bending and torsional moments at G and G' are:

$$\begin{cases} M_{GN} = X_1\sin\gamma - \dfrac{PR}{4}\sin\gamma \\ M_{GT} = -X_1\cos\gamma - \dfrac{PR}{4}(1-\cos\gamma) \\ M_{G'N} = X_1\sin\left(\dfrac{\pi}{2}-\gamma\right) - \dfrac{PR}{4}\sin\left(\dfrac{\pi}{2}-\gamma\right) \\ M_{G'T} = -X_1\cos\left(\dfrac{\pi}{2}-\gamma\right) - \dfrac{PR}{4}(1-\cos\left(\dfrac{\pi}{2}-\gamma\right) \end{cases} \tag{11}$$

Where

$$X_1 = -\frac{\Delta_{1P}}{\Delta_{11}} \tag{12}$$

and

$$\gamma \approx \frac{g}{2R} \tag{13}$$

3.3 Two degrees of freedom models inspired by structural design and static simulation (models 2 and 3)

3.3.1 Expressions of internal displacement

$$\Delta_{D1} = \Delta_{D2} = 0$$

From the above, it follows that in the vertical section passing through D, more than one indeterminate unknown must be introduced so as to ensure the non-effective rotation due to the applied external load $\boldsymbol{Q}$.

Henceforth, let's study a slotted spring under load $\boldsymbol{Q}$ modeled by a structure of two degrees of freedom quarter beam with statically indeterminate structures.

We assume that:

a) Strains in the two directions of the vertical plane sections of the springs are negligible nearby the point D.

b) Displacements due to shear forces are negligible.

c) The behaviour of the spring under applied load verifies the Saint Venant's static hypothesis according to which for a plane section sufficiently far from the application point of the external forces, the effect of the given load can be replaced by an equivalent couple force-torque.
The mentioned above very light rotation of the point D in the two main horizontal and vertical directions may be due to some internal torques $\boldsymbol{X_D}$ and $\boldsymbol{Y_D}$ compensating the effect of the torsion displacement supposed to be caused by the external load (Fig. 5a,b). This corresponds to the primary system (Fig. 5b, c).

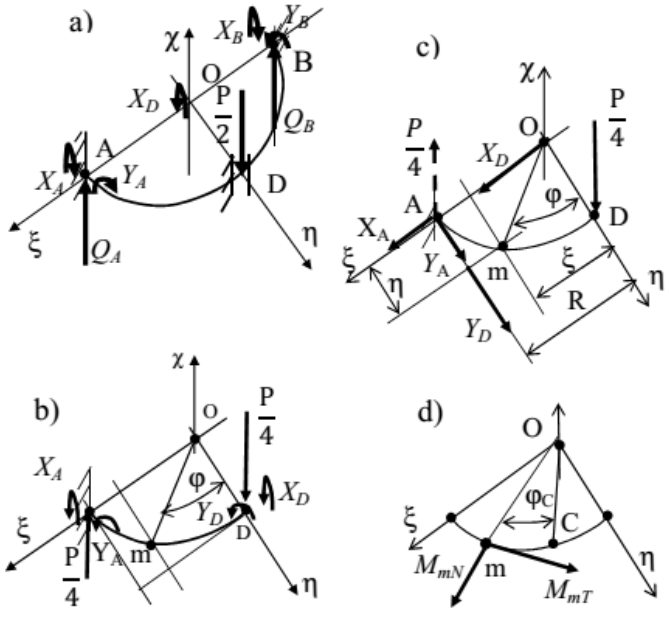

Fig. 5 Internal and external loads in a two d.o.f primary system of the spring ring

Let's add to the symbol of displacement δ and to that of the unknowns $\boldsymbol{X, Y, \ldots}$ the indexes D and C corresponding to their respective values at these points. It is recalled that indexes N and T denote the radial (bending) and tangential (torsional) components. From the conditions of double symmetry, $Q_A = Q_D = P/4$.

We come to the following compatibility equations:

$$\begin{cases} \delta_{D11}X_D + \delta_{D12}Y_D + \delta_{D1Q} = \Delta_{D1} \\ \delta_{D21}X_D + \delta_{D22}Y_D + \delta_{D2Q} = \Delta_{D2} \end{cases} \tag{14}$$

$$\begin{cases} \delta_{C11}X_D + \delta_{C12}Y_D + \delta_{C1Q} = \Delta_{C1} \\ \delta_{C21}X_D + \delta_{C22}Y_D + \delta_{C2Q} = \Delta_{C2} \end{cases} \tag{15}$$

- **Calculation of the unknown internal loads**

1) Unit load internal reaction at a given point of the ring neutral axis m(R,φ).
The moments $\boldsymbol{M_{XD}}$ and $\boldsymbol{M_{YD}}$ due to the internal unknown loads $\boldsymbol{X_D}$ and $\boldsymbol{Y_D}$ at m(R,φ) are made of their decomposition into bending and torsional components defined (Fig. 5.a):

$$\begin{cases} M_{XDN} = X_D \sin\varphi \\ M_{XDT} = -X_D \cos\varphi \\ M_{YDN} = Y_D \cos\varphi \\ M_{YDT} = Y_D \sin\varphi \end{cases} \tag{16}$$

2) Calculation of displacements due to the unit unknown loads:

$$\delta_{D11} = \frac{1}{EI_g}\int_0^{\gamma}\left(\frac{\partial M_{XDN}}{\partial X_D}\right)^2 R\mathrm{d}\varphi + \frac{1}{EI}\int_{\gamma}^{\frac{\pi}{2}-\gamma}\left(\frac{\partial M_{XDN}}{\partial X_D}\right)^2 R\mathrm{d}\varphi + \ldots + \frac{1}{C}\int_0^{\frac{\pi}{2}-\gamma}\left(\frac{\partial M_{XT}}{\partial X_D}\right)^2 R\mathrm{d}\varphi + \frac{1}{C_g}\int_0^{\frac{\pi}{2}}\left(\frac{\partial M_{XDT}}{\partial X_D}\right)^2 R\mathrm{d}\varphi \tag{17}$$

$$\delta_{D22} = \frac{1}{EI_g}\int_0^{\gamma}\left(\frac{\partial M_{YDN}}{\partial Y_D}\right)^2 R\mathrm{d}\varphi + \frac{1}{EI}\int_{\gamma}^{\frac{\pi}{2}-\gamma}\left(\frac{\partial M_{YDN}}{\partial Y_D}\right)^2 R\mathrm{d}\varphi + \ldots + \frac{1}{C}\int_0^{\frac{\pi}{2}-\gamma}\left(\frac{\partial M_{YT}}{\partial Y_D}\right)^2 R\mathrm{d}\varphi + \frac{1}{C_g}\int_0^{\frac{\pi}{2}}\left(\frac{\partial M_{YT}}{\partial Y_D}\right)^2 R\mathrm{d}\varphi \tag{18}$$

$$\delta_{D12} = \frac{1}{EI_g}\int_0^{\gamma}\frac{\partial M_{XDN}}{\partial X_D}\frac{\partial M_{YDN}}{\partial Y_D} R\mathrm{d}\varphi + \frac{1}{EI}\int_{\gamma}^{\frac{\pi}{2}-\gamma}\frac{\partial M_{XDN}}{\partial X_D}\frac{\partial M_{YDN}}{\partial Y_D} R\mathrm{d}\varphi + \ldots + \frac{1}{C}\int_{\frac{\pi}{2}-\gamma}^{\frac{\pi}{2}}\frac{\partial M_{XDT}}{\partial X_{DT}}\frac{\partial M_{YDN}}{\partial Y_D} R\mathrm{d}\varphi \tag{19}$$

3) Internal reaction due to the external load $\boldsymbol{Q}$ in the primary system (Fig. 5.b.c)
By analogy with (7-10) have:

$$\begin{cases} M_{DQN} = -\dfrac{PR}{4}\sin\varphi \\ M_{DQT} = \dfrac{PR}{4}\left(1-\cos\varphi\right) \end{cases} \tag{20}$$

4) Calculation of displacements due to the external loads

$$\delta_{D1Q} = -\left(\frac{1}{EI_g}\int_0^{\gamma} M_{DQN}\frac{\partial M_{XDN}}{\partial X_D}R\mathrm{d}\varphi + \frac{1}{EI}\int_{\gamma}^{\frac{\pi}{2}-\gamma} M_{DQN}\frac{\partial M_{XDN}}{\partial X_D}R\mathrm{d}\varphi + \ldots + \frac{1}{C_g}\int_0^{\frac{\pi}{2}} M_{DQT}\frac{\partial M_{XDT}}{\partial X_D}R\mathrm{d}\varphi \right) \tag{21}$$

$$\delta_{D2Q} = -\left(\frac{1}{EI_g}\int_0^{\gamma} M_{DQN}\frac{\partial M_{YDN}}{\partial Y_D}R\mathrm{d}\varphi + \frac{1}{EI}\int_{\gamma}^{\frac{\pi}{2}-\gamma} M_{DQN}\frac{\partial M_{YDN}}{\partial Y_D}R\mathrm{d}\varphi + \ldots + \frac{1}{C_g}\int_0^{\frac{\pi}{2}} M_{DQT}\frac{\partial M_{YDN}}{\partial Y_D}R\mathrm{d}\varphi \right) \tag{22}$$

3.3.2 Case I: $\Delta_{D1} = \Delta_{D2} = 0$

Naturally, $\Delta_{D2} = 0$. In reality, as it was said above, the angle of rotation Δ_{D1} is very small; nevertheless it is not different from 0. This condition will be taken into account in the in case II. From the system of equations (14), we obtain:

$$\begin{bmatrix} \delta_{D11} & \delta_{D12} \\ \delta_{D12} & \delta_{D22} \end{bmatrix} x \begin{pmatrix} X_D \\ Y_D \end{pmatrix} = \begin{pmatrix} -\delta_{D1Q} \\ -\delta_{D2Q} \end{pmatrix}$$

$$\Rightarrow \begin{pmatrix} X_D \\ Y_D \end{pmatrix} = \begin{pmatrix} \dfrac{-\delta_{D12}\delta_{D2Q} + \delta_{D22}\delta_{1Q}}{\delta_{D22}\delta_{D11} - {\delta_{D12}}^2} \\ \dfrac{-\delta_{D12}\delta_{1Q} + \delta_{D11}\delta_{2Q}}{\delta_{D22}\delta_{D11} - {\delta_{D22}}^2} \end{pmatrix} \tag{23}$$

Finally, the total bending and torsional moments at given point m(φ)

$$\begin{cases} M_{mN} = X_D\sin\varphi + Y_D\cos\varphi - \dfrac{PR}{4}\sin\varphi \\ M_{mT} = X_D\cos\varphi + Y_D\sin\varphi + \dfrac{PR}{4}\left(1-\cos\varphi\right) \end{cases} \tag{24}$$

In particular, at D we have:

$$\begin{cases} M_{DN} = Y_D - \dfrac{PR}{4} \\ M_{DT} = X_D + \dfrac{PR}{4} \end{cases} \tag{25}$$

3.3.3 Case II: $\Delta_{D1} \neq 0$, $\Delta_{C2} \neq 0$

Let's form a mental image of the ring as a fully determinate system where all the above well-defined loads are taken as external loads. In order to determine the unknowns X_D and Y_D, let's write the system of equations corresponding to the application of unit new unknown bending and torsional loads $X_{CN} = 1$ and $Y_{CN} = 0$ at point C. This strategy is the same as that which consist of finding the internal loads at point C by cutting the ring beam. Taking Δ_{D1} and Δ_{C2} as new unknowns, we can use as boundary conditions the equations:

$$\begin{cases} \Delta_{D2} = 0 \\ \Delta_{C1} = 0 \\ \Delta_{D1} \neq 0 \\ \Delta_{C2} \neq 0 \end{cases} \tag{26}$$

Noticing that for the point C, $\varphi = \pi/4$, by analogy to (24):

$$\begin{cases} M_{CN} = X_D\sin\dfrac{\pi}{4} + Y_D\cos\dfrac{\pi}{4} - \dfrac{PR}{4}\sin\dfrac{\pi}{4} \\ M_{CT} = X_D\cos\dfrac{\pi}{4} + Y_D\sin\dfrac{\pi}{4} + \dfrac{PR}{4}\left(1-\cos\dfrac{\pi}{4}\right) \end{cases}$$

$$\Rightarrow \begin{cases} M_{CN} = \dfrac{\sqrt{2}}{2}\left(X_D + Y_D - \dfrac{PR}{4}\right) \\ M_{CT} = \dfrac{\sqrt{2}}{2}\left(X_D + Y_D\right) + \dfrac{PR}{4}\left(1-\dfrac{\sqrt{2}}{2}\right) \end{cases} \tag{27}$$

Noticing that for $\varphi_C = 0$ and by analogy to (24):

$$\begin{cases} M_{mN} = X_C\sin\varphi_C + Y_C\cos\varphi_C - \dfrac{PR}{4}\sin\varphi_C \\ M_{mT} = X_C\cos\varphi_C + Y_C\sin\varphi_C + \dfrac{PR}{4}\left(1-\cos\varphi_C\right) \end{cases} \tag{28}$$

$$\Rightarrow \begin{cases} M_{CN} = Y_C \\ M_{CT} = X_C \end{cases} \tag{29}$$

On the whole, from (14), (16), (46), (29), we obtain the following system of 6 equations:

$$\begin{cases} \delta_{D11}X_D + \delta_{D12}Y_D - \Delta_{D1} = -\delta_{D1Q} \\ \delta_{D21}X_D + \delta_{D22}Y_D = -\delta_{D2Q} \\ \delta_{C11}X_C + \delta_{C12}Y_C + \delta_{C1Q'} = 0 \\ \delta_{C21}X_C + \delta_{C22}Y_C + \delta_{C2Q'} = \Delta_{C2} \\ \dfrac{\sqrt{2}}{2}X_D + \dfrac{\sqrt{2}}{2}Y_D - X_C + \dfrac{PR}{4}\left(1-\dfrac{\sqrt{2}}{2}\right) = 0 \\ \dfrac{\sqrt{2}}{2}X_D + \dfrac{\sqrt{2}}{2}Y_D - Y_C = 0 \end{cases} \tag{30}$$

In which

$$\begin{cases} M_{CQ'N} = \left(-\dfrac{PR}{4}\right)\sin\varphi + X_D\sin\varphi + Y_D\cos\varphi \\ M_{CQ'T} = \left(-\dfrac{PR}{4}\right)\cos\varphi - X_D\cos\varphi + Y_D\sin\varphi \end{cases} \tag{31}$$

Where $\boldsymbol{Q'}$ is the result of loads applied at D in the previous primary system.

We have:

$$\delta_{C11}=\frac{1}{EI_g}\int_0^{\gamma}\frac{\partial M_{XCN}}{\partial X_C}^2 R\mathrm{d}\varphi_C+\frac{1}{EI}\int_{\gamma}^{\frac{\pi}{2}-\gamma}\frac{\partial M_{XCN}}{\partial X_C}^2 R\mathrm{d}\varphi_C+\ldots$$
$$+\frac{1}{C}\int_0^{\frac{\pi}{2}-\gamma}\frac{\partial M_{XCT}}{\partial X_C}^2 R\mathrm{d}\varphi_C+\frac{1}{C_g}\int_0^{\frac{\pi}{2}}\frac{\partial M_{XCT}}{\partial X_C}^2 R\mathrm{d}\varphi_C \tag{32}$$

$$\delta_{C22}=\frac{1}{EI_g}\int_0^{\gamma}\frac{\partial M_{YCN}}{\partial Y_C}^2 R\mathrm{d}\varphi_C+\frac{1}{EI}\int_{\gamma}^{\frac{\pi}{2}-\gamma}\frac{\partial M_{YCN}}{\partial Y_C}^2 R\mathrm{d}\varphi_C+\ldots$$
$$+\frac{1}{C}\int_0^{\frac{\pi}{2}-\gamma}\frac{\partial M_{YCN}}{\partial Y_C}^2 R\mathrm{d}\varphi_C+\frac{1}{C_g}\int_0^{\frac{\pi}{2}}\frac{\partial M_{YCN}}{\partial Y_D}^2 R\mathrm{d}\varphi_C \tag{33}$$

$$\delta_{C1Q}=-\left(\frac{1}{EI_g}\int_0^{\gamma}M_{QN}\frac{\partial M_{XCN}}{\partial X_{CN}}R\mathrm{d}\varphi_C\right)$$
$$\left(+\frac{1}{EI}\int_{\gamma}^{\frac{\pi}{2}-\gamma}M_{Q'N}\frac{\partial M_{XCN}}{\partial X_{CN}}R\mathrm{d}\varphi_C+\ldots+\frac{1}{C_g}\int_0^{\frac{\pi}{2}}M_{Q'T}\frac{\partial M_{XCT}}{\partial X_{CT}}R\mathrm{d}\varphi_C\right)$$
$$-\left(\frac{1}{EI_g}\int_0^{\gamma}X_{DN}\frac{\partial M_{XCN}}{\partial X_C}R\mathrm{d}\varphi_C\right)$$
$$\left(+\frac{1}{EI}\int_{\gamma}^{\frac{\pi}{2}-\gamma}X_{DN}\frac{\partial M_{XCN}}{\partial X_C}R\mathrm{d}\varphi_C+\ldots+\frac{1}{C_g}\int_0^{\frac{\pi}{2}}X_{DT}\frac{\partial M_{XCT}}{\partial X_C}R\mathrm{d}\varphi_C\right)$$
$$-\left(\frac{1}{EI_g}\int_0^{\gamma}Y_{DN}\frac{\partial M_{XCN}}{\partial X_C}R\mathrm{d}\varphi_C+\frac{1}{EI}\int_{\gamma}^{\frac{\pi}{2}-\gamma}Y_{DN}\frac{\partial M_{XCN}}{\partial X_C}R\mathrm{d}\varphi_C+\cdots\right)$$
$$\left(+\frac{1}{C_g}\int_0^{\frac{\pi}{2}}Y_{DT}\frac{\partial M_{XCT}}{\partial X_C}R\mathrm{d}\varphi_C\right) \tag{34}$$

$$\delta_{C2Q'}=-\left(\frac{1}{EI_g}\int_0^{\gamma}M_{QN}\frac{\partial M_{YCN}}{\partial Y_C}R\mathrm{d}\varphi_C+\frac{1}{EI}\int_{\gamma}^{\frac{\pi}{2}-\gamma}M_{Q'N}\frac{\partial M_{YCN}}{\partial Y_C}R\mathrm{d}\varphi_C\right)$$
$$\left(+\ldots+\frac{1}{C_g}\int_0^{\frac{\pi}{2}}M_{Q'T}\frac{\partial M_{YCT}}{\partial Y_C}R\mathrm{d}\varphi_C\right)$$
$$-\left(\frac{1}{EI_g}\int_0^{\gamma}X_{DN}\frac{\partial M_{YCN}}{\partial Y_C}R\mathrm{d}\varphi_C+\frac{1}{EI}\int_{\gamma}^{\frac{\pi}{2}-\gamma}X_{DN}\frac{\partial M_{YCN}}{\partial Y_C}R\mathrm{d}\varphi_C\right)$$
$$\left(+\ldots+\frac{1}{C_g}\int_0^{\frac{\pi}{2}}X_{DT}\frac{\partial M_{YCT}}{\partial Y_C}R\mathrm{d}\varphi_C\right)-\left(\frac{1}{EI_g}\int_0^{\gamma}Y_{DN}\frac{\partial M_{YCN}}{\partial Y_C}R\mathrm{d}\varphi_C\right)$$
$$\left(+\frac{1}{EI}\int_{\gamma}^{\frac{\pi}{2}-\gamma}Y_{DN}\frac{\partial M_{YCN}}{\partial Y_C}R\mathrm{d}\varphi_C+\ldots+\frac{1}{C_g}\int_0^{\frac{\pi}{2}}Y_{DT}\frac{\partial M_{YCT}}{\partial Y_C}R\mathrm{d}\varphi_C\right) \tag{35}$$

The bending and torsional components $\boldsymbol{M_{XC}}$ and $\boldsymbol{M_{YC}}$ of the internal unknown loads $\boldsymbol{X_C}$ and $\boldsymbol{Y_C}$ at m(R,φ_C) are defined on (Fig. 6.a):

$$\begin{cases}M_{XCN}=X_C\sin\varphi_C\\ M_{XCT}=-X_C\cos\varphi_C\\ M_{YCN}=Y_C\cos\varphi_C\\ M_{YCT}=Y_C\sin\varphi_C\end{cases} \tag{36}$$

From (34) and (35) we can note:

$$\delta_{C1Q'}=\delta_{C1Q}+b_1X_D+c_1Y_D$$

$$\delta_{C2Q'}=\delta_{C2Q}+b_2X_D+c_2Y_D$$

Where b_1, b_2, c_1 and c_2 are calculated coefficients.

Then (30) and (31) becomes:

$$\begin{cases}\delta_{D12}X_D+\delta_{D22}Y_D=-\delta_{D2Q}\\ b_1X_D+c_1Y_D+\delta_{C11}X_C+\delta_{C12}Y_C=-\delta_{C1Q}\\ \frac{\sqrt{2}}{2}X_D+\frac{\sqrt{2}}{2}Y_D-X_C=-\frac{PR}{4}\left(1-\frac{\sqrt{2}}{2}\right)\\ \frac{\sqrt{2}}{2}X_D+\frac{\sqrt{2}}{2}Y_D-Y_C=\frac{\sqrt{2}}{8}PR\\ \delta_{D11}X_D+\delta_{D12}Y_D-\Delta_{D1}=-\delta_{D1Q}\\ b_2X_D+c_2Y_D+\delta_{C21}X_C+\delta_{C22}Y_C-\Delta_{C2}=-\delta_{C2Q}\end{cases} \tag{37}$$

Expressions δ_{11}, δ_{1Q}, δ_{D11}, δ_{D12}, δ_{D22}, δ_{Q1}, δ_{Q2}, δ_{C11}, δ_{C12}, δ_{C22}, δ_{CQ1}, b_1, c_1, b_2 and c_2 are gathered in Table 1.

3.4 General case of *n* slots per section springs

The symmetrical and antisymmetrical properties of structural systems are usually taken into consideration in order to facilitate their analysis as statically indeterminate systems. The *n* per section slotted cylinder springs has *n*-times multiple geometrical, cross-section and physical data symmetries. This allows limiting their studies to that of π/n^{th} fragment of the spring. Therefore, the corresponding expressions are obtained by replacing in the Eqs. (18)-(22) the number $\pi/2$ by π/n. For instance:

$$\delta_{11}=\frac{1}{EI_g}\int_0^{\gamma}X_{1N}{}^2R\mathrm{d}\varphi+\frac{1}{EI}\int_{\gamma}^{\frac{\pi}{n}-\gamma}X_{1N}{}^2R\mathrm{d}\varphi+\cdots$$
$$+\frac{1}{C_g}\int_0^{\gamma}X_{1T}{}^2R\mathrm{d}\varphi+\frac{1}{C}\int_{\gamma}^{\frac{\pi}{2}-\gamma}X_{1T}{}^2R\mathrm{d}\varphi+\frac{1}{C_g}\int_{\frac{\pi}{n}-\gamma}^{\frac{\pi}{2}}X_{1T}{}^2R\mathrm{d}\varphi \tag{38}$$

4 Numerical application and discussion

4.1 Flowchart for comparison in Excel

Static simulation was made on the basis of models created in Solidworks. This software modelling exploits finite elements

Table 1 Summary of expressions of displacements under unit loads

FIRST Model

$$\delta_{11} \quad \frac{R}{2EI_g}\left(\gamma-\frac{1}{2}\right)\sin(2\gamma)+\frac{R}{2C_g}\left(\gamma+\frac{1}{2}\sin(2\gamma)\right)+\frac{R}{2EI}\left(\frac{\pi}{4}-\frac{1}{2}-\gamma+\frac{1}{2}\sin(2\gamma)\right)+\frac{R}{2C}\left(\frac{\pi}{4}+\frac{1}{2}-\gamma-\frac{1}{2}\sin(2\gamma)\right) \tag{39}$$

$$-\delta_{1P} \quad \frac{PR^2}{8EI_g}\left(\gamma-\frac{1}{2}\right)\sin(2\gamma)+\frac{PR^2}{8EI}\left(\frac{\pi}{4}-\frac{1}{2}-\gamma+\frac{1}{2}\sin(2\gamma)\right)+\frac{PR^2}{4C_g}\left(-\sin\ \gamma+\frac{1}{2}\gamma+\frac{1}{4}\sin(2\gamma)\right)+\frac{PR^2}{4C}\left(\sin\ \gamma-\frac{1}{4}\sin(2\gamma)-\frac{1}{2}\gamma-\frac{1}{2}\gamma+\frac{1}{4}-\frac{\sqrt{2}}{2}-\frac{\pi}{8}\right) \tag{40}$$

SECOND Model

$$\begin{matrix}\delta_{12}\\ =\delta_{21}\end{matrix} \quad R\gamma\left(\frac{1}{EI_g}+\frac{1}{C_g}\right)+\frac{R}{2}\left(\frac{\pi}{2}-2\gamma\right)\left(\frac{1}{EI}+\frac{1}{C}\right) \tag{41}$$

$$\begin{matrix}\delta_{11}\\ =\delta_{22}\end{matrix} \quad \frac{R}{2}\left(1-\cos(2\gamma)\right)\left(\frac{1}{EI_g}-\frac{1}{C_g}\right)+\frac{R}{2}\cos(2\gamma)\left(\frac{1}{EI}-\frac{1}{C}\right) \tag{42}$$

$$-\delta_{1Q} \quad \frac{PR^2}{4EI_g}\gamma+\frac{PR^2}{4EI}\left(\frac{\pi}{4}-\gamma\right)+\frac{PR^2}{4C_g}\left(\sin\ \gamma-\cos\ \gamma-\gamma+1\right)+\frac{PR^2}{4C}\left(\cos\ \gamma-\sin\ \gamma-\frac{\pi}{4}\gamma+\gamma\right) \tag{43}$$

$$-\delta_{2Q} \quad \frac{PR^2}{8EI_g}\left(1-\cos(2\gamma)\right)+\frac{PR^2}{8EI}\cos(2\gamma)+\frac{PR^2}{4C_g}\left(\cos\ \gamma-\sin\ \gamma-\frac{1}{2}\cos(2\gamma)-\frac{1}{2}\right)+\frac{PR^2}{4C}\left(\sin\ \gamma-\cos\ \gamma+\frac{1}{2}\cos(2\gamma)\right) \tag{44}$$

THIRD Model

$$\delta_{c11} \quad \frac{R}{4}\left[\frac{1}{EI_g}\left(-1+2\gamma+\cos 2\gamma\right)+\frac{1}{EI}\left(\frac{\pi}{2}-2\gamma-\cos 2\gamma\right)+\frac{1}{C_g}\left(1+2\gamma-\cos 2\gamma\right)+\frac{1}{C}\left(\frac{\pi}{2}-2\gamma+\cos 2\gamma\right)\right] \tag{45}$$

$$\delta_{c12} \quad \frac{R}{4}\left[\frac{1}{EI_g}\sin 2\gamma+\frac{1}{EI}\left(1-\sin 2\gamma\right)-\frac{1}{C_g}\sin 2\gamma-\frac{1}{C}\left(1-\sin 2\gamma\right)\right] \tag{46}$$

$$\delta_{c22} \quad \frac{R}{4}\left[\frac{1}{EI_g}\left(1+2\gamma-\cos 2\gamma\right)+\frac{1}{EI}\left(\frac{\pi}{2}-2\gamma+\cos 2\gamma\right)+\frac{1}{C_g}\left(-1+2\gamma+\cos 2\gamma\right)+\frac{1}{C}\left(\frac{\pi}{2}-2\gamma-\cos 2\gamma\right)\right] \tag{47}$$

$$-\delta_{CQ1} \quad \frac{\sqrt{2}R^2}{32}\left[\frac{1}{EI_g}\left(-2+4\gamma+2\cos 2\gamma+2\sin 2\gamma\right)+\frac{1}{EI}\left(\pi+2-4\gamma-2\sin 2\gamma-2\cos 2\gamma\right)+\frac{1}{C_g}\left(3-4\gamma-8\left(\cos\ \gamma-\sin 2\gamma\right)+2\cos 2\gamma+2\sin 2\gamma\right)\right.$$
$$\left.+\frac{1}{C}\left(-\pi+2+4\gamma+8\left(\sin\ \gamma-\sin\ \gamma\right)-2\sin 2\gamma-2\sin 2\gamma\right)\right] \tag{48}$$

$$b_1 \quad -\frac{R\sqrt{2}}{16}\left[\frac{1}{EI_g}\left(-2+4\gamma+2\sin 2\gamma+2\cos 2\gamma\right)+\frac{1}{EI}\left(\pi+2-4\gamma-2\sin 2\gamma-2\cos 2\gamma\right)+\frac{1}{C_g}\left(2+4\gamma-2\cos 2\gamma-2\sin\gamma\right)+\frac{1}{C}\left(\pi-2-4\gamma+2\sin 2\gamma+2\cos 2\gamma\right)\right] \tag{49}$$

$$c_1 \quad \frac{R\sqrt{2}}{16}\left[\frac{1}{EI_g}\left(2-4\gamma+2\sin 2\gamma-2\cos 2\gamma\right)+\frac{1}{EI}\left(-\pi+2+4\gamma-2\sin 2\gamma+2\cos 2\gamma\right)+\frac{1}{C_g}\left(-2-4\gamma-2\sin 2\gamma+2\cos 2\gamma\right)+\frac{1}{C}\left(-\pi-2+4+2\sin 2\gamma-2\cos 2\gamma\right)\right] \tag{50}$$

$$-\delta_{CQ2} \quad \frac{\sqrt{2}PR^2}{16}\left[\frac{1}{EI_g}\left(\frac{1}{2}++\frac{1}{2}\sin 2\gamma-\frac{1}{2}\cos 2\gamma\right)+\frac{1}{EI}\left(\frac{\pi}{4}+\frac{1}{2}-\gamma-\frac{1}{2}\sin 2\gamma+\frac{1}{2}\cos 2\gamma\right)-\frac{1}{C_g}\left(-\frac{5}{2}+\gamma+2\left(\sin 2\gamma+\cos 2\gamma\right)-\frac{1}{2}\sin 2\gamma+\frac{1}{2}\cos 2\gamma\right)\right.$$
$$\left.-\frac{1}{C}\left(\frac{\pi}{4}-\gamma+2\sqrt{2}-\frac{1}{2}-2\left(\cos\ \gamma+\sin\ \gamma\right)\frac{1}{2}\sin 2\gamma-\frac{1}{2}\cos 2\gamma\right)\right] \tag{51}$$

$$b_2 \quad \frac{R\sqrt{2}}{16}\left[\frac{1}{EI_g}\left(2+4\gamma-2\sin 2\gamma+2\cos 2\gamma\right)+\frac{1}{EI}\left(\pi+2-4\gamma-2\sin 2+2\cos 2\right)+\frac{1}{C_g}\left(-2+4\gamma-2\sin 2\gamma+2\cos 2\gamma\right)+\frac{1}{C}\left(\pi-2-4\gamma+2\sin 2\gamma-2\cos 2\gamma\right)\right] \tag{52}$$

$$c_2 \quad \frac{R\sqrt{2}}{16}\left[\frac{1}{EI_g}\left(2+4\gamma-2\sin 2\gamma-2\cos 2\gamma\right)+\frac{1}{EI}\left(\pi-2-4\gamma+2\sin 2+2\cos 2\right)+\frac{1}{C_g}\left(-2+4\gamma+2\sin 2\gamma+2\cos 2\gamma\right)+\frac{1}{C}\left(\pi+2-4\gamma-2\sin 2\gamma-2\cos 2\gamma\right)\right] \tag{53}$$

numerical application. It allows to generate meshes and provides graphical presentation of the displacements and stresses related to given design parameters and loads. Provided that the simulation accuracy is a function of the mesh density, standard parameters and finest mesh were chosen in order that results may not be significantly affected by the error of discretization.

In order to compare one with another the different models, a program on the basis of a flowchart (Fig. 6) is elaborated and introduced in Excel. The basic data are the same as that of a previous works [6] (Table 2). Tables 3-6 give the results of the calculation of the stress values respectively for the first, the second and the third newly proposed models.

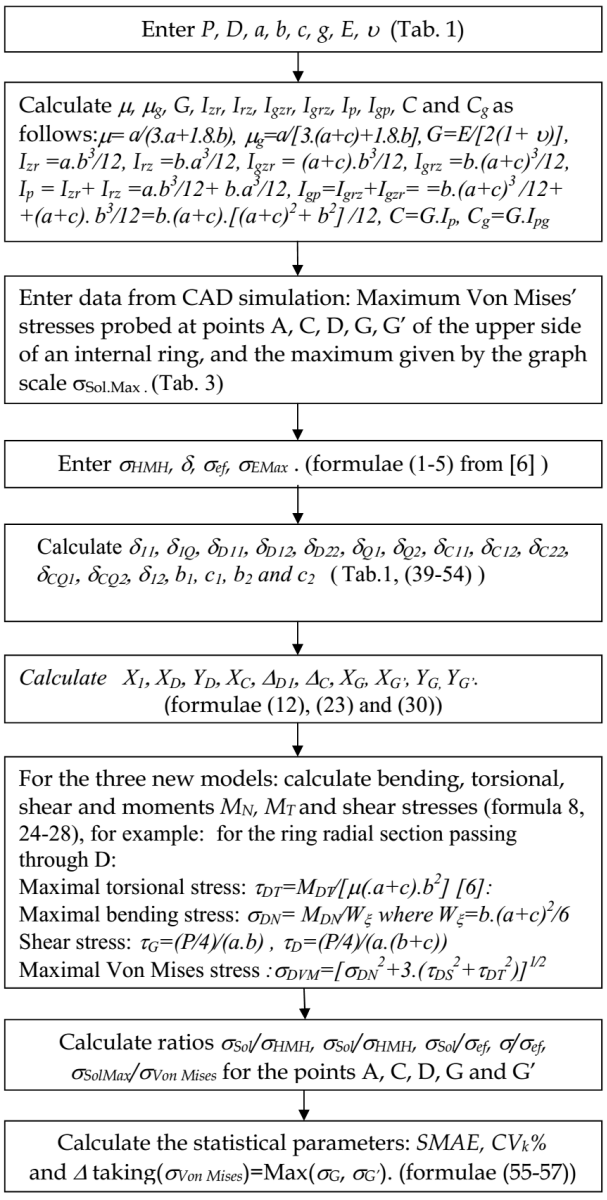

Fig. 6 Flowchart for calculation

When confronted with multiple measurements $y_1, y_2, y_3, \ldots$ of the same experiment, one typically reports at least two properties of the set of scores, namely:

The scaled mean absolute error (SMAE) of the stress ratio:

Table 2 Basic data

No	External load	Nominal diameter	Spring diameter	Spring width	Ring heigth	Slot width
	P [N]	D_N [m]	D [m]	b [m]	a [m]	c [m]
1	2000	0.015	0.02	0.005	0.003	0.003
2	2000	0.015	0.02	0.005	0.003	0.003
3	2000	0.015	0.02	0.005	0.003	0.002
4	500	0.019	0.02	0.001	0.003	0.003
5	500	0.018	0.02	0.002	0.003	0.003
6	2000	0.017	0.02	0.003	0.003	0.003
7	2000	0.016	0.02	0.004	0.003	0.003
8	500	0.014	0.015	0.001	0.003	0.002
9	500	0.0135	0.015	0.0015	0.003	0.002
10	1000	0.0225	0.025	0.0025	0.003	0.002
11	2000	0.0195	0.025	0.0055	0.003	0.002

$$SMAE = \frac{1}{nA}\sum_{i=1}^{n}\left|y_i - A\right| = \frac{1}{n}\sum_{i=1}^{n}\left|\frac{\sigma_{Gi}}{\sigma_{G'i}} - 1\right| \tag{54}$$

The coefficient of variation (CV) -standard deviation of the stress ratio: provides a scaled measure of precision

$$\begin{aligned} CV_k\% &= \frac{100}{\bar{y}} SD\% = \frac{100}{\bar{y}}\sqrt{\left[\sum_{i=1}^{n-1}\frac{(y_i-\bar{y})^2}{n-1}\right]}\% \\ &= \frac{100}{\bar{y}}\sqrt{\left[\sum_{i=1}^{n-1}\frac{1}{n-1}\left(\frac{\sigma_{Gi}}{\sigma_{G'i}}-\bar{y}\right)^2\right]}\% \end{aligned} \tag{55}$$

Let's add the maximum difference stress ratio:

$$\Delta_i = \max\left(y_i\right) - \max\left(y_j\right) \tag{56}$$

where A is the ideal ratio, and ȳ and *SD* the absolute mean and the standard deviation. The Von Mises' stress values σ_{Gi} and $\sigma_{G'i}$ of the previous and proposed models are to be compared one with another in term of accuracy and precision respectively by means of [18].

4.2 Main results and discussion

a) One can probe and calculate the angle of rotation of the ring symmetrical planes passing through C and D about tangential axes respectively by the formula:

$$\Delta_D \cong \frac{\delta_{Dext} - \delta_{dext}}{2a} - \frac{\delta_{D\,\mathrm{int}} - \delta_{d\,\mathrm{int}}}{2a} \;,\; \Delta_C \cong \frac{\delta_{Cext} - \delta_{cext}}{2a} - \frac{\delta_{C\,\mathrm{int}} - \delta_{c\,\mathrm{int}}}{2a} \tag{57}$$

where δ refers to the vertical displacements, D, C, respectively d and c to the ring upper and lower surfaces, and the indexes ext and int to the external and internal ring sides in the simulation graphics. At point D, Δ_D is too small for the rotation around X_1 direction and is equal to zero around η axis. On the contrary Δ_C is equal to zero for

the rotation around the tangential axis passing through C. For a reason of a lack of precision of the measurement equipment of the test bench and the Solidworks simulation probe tools, precise values of Δ_{D1} and Δ_{C2} couldn't be obtained since the order of magnitude of the obtained values are comparable with the measurement and calculation errors. Hence we could not consider them. However, more precise values analytically calculated are presented in Table 3.

b) An extract of the main results of the static simulation and studied models is given in Table 4 for some particular points. The calculated ratios and their statistic quantities are shown in Table 5. Deduced from it, Table 6 presents a classification of models firstly relatively to Rivin's experimental formula and secondly relatively to data from static solidworks simulation.

c) For the fillet radius $r = 0$, the distribution of Von Mises' stresses at the ring sections passing through points G and G' is very complex (Fig. 3c). The point of maximum value is located approximately at the inside ring-support contact point belonging to ring radial section passing through G or G'. Practically we have,

$$\sigma_{E\max} \approx \max\left(\sigma_{G\,\mathrm{int}},\ \sigma_{EG'\,\mathrm{int}}\right)$$

On the one hand, these stresses are different for two points located symmetrically relatively to the neutral horizontal plane. On the other hand, they have the same value for points located on either sides and belonging to opposite supports.

d) The first position of the third model in the comparison with solidworks (Table 6) confirms the hypothesis on the basis of which this model is built and the well-founded of the consideration of the rotation of the point D (or D section) around η axis. Its higher position compared to that of the second model confirms that although the torsional deflection of the application point D is small, it is worth not neglecting it.

e) For the fillet radius $r = c$, given by the arc EE' (Fig. 3f), the point of the Von Mises maximum value is no longer situated in the ring section passing through points G or G', but approximately at the inner point G''of the bottom quarter of the fillet arc. Compared to the precedent values the percent error for the maximum Von Mises' stresses have increased irregularly as a function of each of spring parameters a, b, c, D, g and r by more than 10% (Table 7) This can be explained by the consequent decrease of stress concentration in the spring.

Table 3 Internal loads and displacements

No	*XD* [N.m]	*YD* [N.m]	*XC* [N.m]	*YC* [N.m]	$\Delta D1$ [rad.]	$\Delta C2$ [rad.]
1	1.5100	0.5474	2.5532	-1.1968	-0.0037	-0.0034
2	1.0572	0.6736	2.2490	-1.5284	-0.0054	-0.0047
3	1.0411	0.5474	2.2216	-1.5284	-0.0054	-0.0055
4	0.1604	-0.1709	0.3404	-0.8471	-0.0180	-0.0190
5	0.2004	-0.0789	0.4154	-0.7096	-0,0072	-0.0082
6	0.9665	0.0656	1.9746	-2.2754	-0.0146	-0.0161
7	1.0832	0.3753	2.2029	-1.7971	-0.0082	-0.0087
8	0.0604	-0.1352	0.2034	-0.6716	-0.0111	-0.0117
9	0.0456	-0.0637	0.1426	-0.3880	-0.0041	-0.0043
10	0.5025	-0.1608	1.0654	-1.7471	-0.0184	-0.0209
11	1.5624	0.7695	3.0768	-1.7982	-0.0077	-0.0078

Table 4 Von Mises' stresses

N^0	Rivin's Empirical Formula	Michalczyk's Theoretical Formula	Ansys Modeling & simulation	SolidWorks Modeling & simulation		Model 1	Model 2			Model 3
						Structural analysis				
	G	G	G	G*	α^0	G and G'	G	G'	G	G'
	σ_{ef} [Pa]	σ_{Emax} [Pa]	σ_{HMNG} [Pa]	σ_{solmax}[Pa]		σ_{solmax}[Pa]	σ_{G2}[Pa]	$\sigma_{G2'}$[Pa]	σ_{G3}[Pa]	$\sigma_{G3'}$[Pa]
1	348000000	513000000	560000000	632852672	0.08	335262073	381753834	562740559	237919873	603385070
2	348000000	477000000	510000000	582047360	0.06	305284544	388696918	558533398	193266731	607382991
3	388000000	667000000	700000000	642282944	0.05	333474239	378422342	556031793	176514796	623174810
4	1852000000	1105999999	1390000000	1694984504	0.31	677318516	1266219609	2233068182	382161118	1913528668
5	517000000	410000000	464000000	574984960	0.1	252601011	390146225	660847083	148185142	624433656
6	999000000	963000000	1105000000	1281839616	0.2	607136106	830190383	1339209689	350134447	1358863683
7	565000000	680000000	785000000	779210048	0.12	432836885	537147015	826372222	247280707	881947140
8	1522000000	1097000000	1255000000	1303347456	0.18	442800079	957439396	1622531064	239826506	1307429028
9	700000000	595000000	500000000	659928128	0.09	243213300	468409803	778424456	127363539	702754634
10	957000000	1008000000	1080000000	1046998976	0.11	234992497	680934798	1151537535	249510536	1155049957
11	403000000	787000000	820000000	679158848	0.04	122441160	432710080	633938036	215494976	727476191

Table 5 Values of Statistical quantities determining the ratio (σ_i/σ_j) for different models

N⁰	Ansys Rivin	Ansys Mich	Ansys Solidw	Michal. Rivin	Solidw Rivin	Michal. Solidw	Rivin Solidw	Model I Rivin	Model 2 Rivin		Model I Solidw.	Model 2 Solidworks		Model 3 Rivin		Model 3 Solidworks	
	G*	G*	G*	G*	G*	G*	G*	G	G	G'	G	G	G'	G	G'	G	G'
1	1.6	1.09	0.88	1.47	1.82	0.81	0.55	0.96	1.10	1.62	0.53	0.60	0.89	0.68	1.73	0.38	0.95
2	1.46	1.07	0.88	1.37	1.67	0.82	0.60	0.88	1.12	1.60	0.52	0.67	0.96	0.56	1.75	0.33	1.04
3	1.8	1.05	1.09	1.72	1.66	1.04	0.60	0.86	0.98	1.43	0.52	0.59	0.87	0.45	1.61	0.27	0.97
4	0.75	1.26	0.82	0.60	0.92	0.65	1.09	0.37	0.68	1.21	0.40	0.75	1.32	0.21	1.03	0.23	1.13
5	0.9	1.13	0.81	0.79	1.11	0.71	0.90	0.49	0.75	1.28	0.44	0.68	1.15	0.29	1.21	0.26	1.09
6	1.1	1.15	0.86	0.96	1.28	0.75	0.78	0.61	0.83	1.34	0.47	0.65	1.04	0.35	1.36	0.27	1.06
7	1.4	1.15	1.01	1.20	1.38	0.87	0.73	0.77	0.95	1.46	0.56	0.69	1.06	0.44	1.56	0.32	1.13
8	0.82	1.14	0.96	0.72	0.86	0.84	1.17	0.29	0.63	1.07	0.34	0.73	1.24	0.16	0.86	0.18	1.00
9	0.7	0.84	0.76	0.85	0.94	0.90	1.06	0.35	0.67	1.11	0.37	0.71	1.18	0.18	1.00	0.19	1.06
10	1.12	1.07	1.03	1.05	1.09	0.96	0.91	0.25	0.71	1.20	0.22	0.65	1.10	0.26	1.21	0.24	1.10
11	2.04	1.04	1.21	1.95	1.69	1.16	0.59	0.30	1.07	1.57	0.18	0.64	0.93	0.53	1.81	0.32	1.07
SMAE	0.40	0.12	0.12	0.35	0.36	0.17	0.24	0.44	0.19	0.35	0.59	0.33	0.13	0.63	0.40	0.73	0.07
CV%	3.28	0.87	1.32	3.41	2.44	1.54	2.49	4.40	1.95	1.33	2.77	0.68	1.25	4.20	2.21	2.01	0.51
Δ_y	1.34	0.42	0.45	1.36	0.96	0.51	0.62	0.72	0.49	0.55	0.38	0.16	0.45	0.53	0.95	0.19	0.18
col. N⁰	*1*	*2*	*3*	*4*	*5*	*6*	*7*	*8*	*9*	*10*	*11*	*12*	*13*	*14*	*15*	*16*	*17*

Table 6 Comparison of the accuracy of different models empirical

Classification based on Rivin's formula						
Order	1	2	3	4	5	6
SMAE	0.35 Model 2	0.35 Michalczyk	0.35 Model.1	0.36 Solidwks	0.40 Model 3	0.40 Ansys
CV_k %	1.33 Model 2	2.21 Model 3	2.44 solidworks	3.28 Ansys	3.41 Michalczyk	4.40 Model 1
Δ_y	0.55 Model 2	0.72 Model 1	0.95 Model 3	0.96 Soldwks	1.34 Ansys	1.36 Mich.
Classification based on Solidworks' data						
SMAE	0.07 Model 3	0,12 Ansys	0.13 Model 2	0.17 Michalczyk	0.24 Rivin	0.59 Model 1
CV_k %	0.51 Model 3	1.25 Model 2	1.32 Ansys	1.54 Michalczyk	2.49 Rivin	2.77 Model 1
Δ_y	0.18 Model 3	0.38 Model 1	0.45 Ansys	0.45 Model 2	0.51 Mich.	0.62 Rivin

Table 7 Comparison of Von Mises stresses for *zero* and *c* fillet radii

N⁰	*r*=0			*r*=*c*			Percent error difference
	Solidworks	Model 3	Percent	Solidworks	Model 3	Percent	
	σsol_{max}	$max(\sigma_G, \sigma_{G'})$	error	σsol_{max}	$max(\sigma_G, \sigma_{G'})$	error	
	[Pa]	[Pa]		[Pa]	[Pa]		
1	632852672	603385070	4.66	573078080	603385070	5.29	0.63
2	582047360	607382991	4.35	504143520	607382991	20.48	16.13
3	642282944	623174810	2.98	670784128	623174810	7.10	4.12
4	1694984504	1913528668	12.89	1318188160	1913528668	45.16	32.71
5	574984960	624443656	8.60	473096608	624443656	31.99	23.39
6	1281833616	1358863683	6.01	1132198784	1358863683	20.02	14.01
7	779210048	881947149	13.18	735811520	881947149	19.86	6.68
8	1303347456	1307429028	0.31	1134831104	1307429028	15.21	14.90
9	659928128	702754634	6.49	585020672	702754634	20.12	13.63
10	1046998976	1155049957	10.32	1026296000	1155049957	12.55	2.33

5 Conclusion and perspectives

In order to facilitate the slotted cylinder spring design, three statistically indeterminate structural mechanics modelling approaches were presented and compared one with others using standard statistical quantities. Assumption according to which "the point of the slotted cylinder spring situated at 45^0 of the symmetrical plane hasn't a relative rotation around the neutral axis, but just moves in the axial direction" was confirmed by CAD modeling. Together with this assumption, the absence of bending deflection at the application point allowed formulating a couple of boundary conditions necessary to solve a linear system of six equations written for the two d.o.f. proposed model. As it was expected, the analysis of the results of calculation based on sample data shows clearly that such model is of higher precision and accuracy. The precision expressed by the Von Mises stress standard deviation is about 2.21% relatively to the experimental data and 0.51% relatively to Solidworks simulation. As perspective, the implementation of the new method in global slotted spring software should allow to calculate the better value of the Von Mises stress as key parameter. It is planned to extend the theory over springs with more than two slots per section and to clarify the analytical relationship between the Von Mises stresses and the radius of the fillet linking the slotted cylinder spring rings and it supports. A large study is foreseen based on experimental plan method in which the failure state and the fracture point or zone of such springs will be observed for a large number of manufactured slotted cylinder springs.

References

[1] Razooqi, A. I., Ameen, H. A., Mashloosh, K. M. "Static and Dynamic Characteristics of Slotted Cylinder Spring." *International Journal of Engineering Research & Techmology*. 2(12), pp. 3860-3871. 2013.

[2] Razooqi, A. I., Ameen, H. A., Mashloosh, K. M. "Compression and impact characterization of helical and slotted cylinder springs." *International Journal of Engineering and Technology.* 3(2), pp. 268-278, 2014. https://doi.org/10.14419/ijet.v3i2.2492

[3] Gnateski, V. "Slotted Spring Vibration Isolator." United States Patent Application Publication, N^0 US 2012/0049422 Al, 2012.

[4] Schneider, W. A. "Design and application of slotted cylinder springs." United States Army, USAELRDL Technical Report 2327, 1963. https://doi.org/10.21236/ad0425207

[5] Rivin, E. I. "*Passive Isolation Vibration*." New York, ASME PRESS, 2003. https://doi.org/10.1115/1.80187x

[6] Michalczyk K. "Stress analysis in slotted springs." *Mechanics*. 25(3), pp. 131-134. 2006.

[7] Saleeb, A. F., Chang, T. Y. "On the hybrid-mixed formulation C0 curved beam elements." *Computer Methods in Applied Mechanical Engineering*. 60(1), pp. 95-121. 1987. https://doi.org/10.1016/0045-7825(87)90131-9

[8] Shi, G., Voyiadjis, G. Z. "Simple and efficient shear flexible two-node arch/beam and four-node cylindrical shell/plate finite elements." *International Journal of Numerical Methods in Engineering*. 31(4), pp. 759-776. 1991. https://doi.org/10.1002/nme.1620310408

[9] Wang, T. M., Merrill, T. F. "Stiffness coefficients of noncircular curved beams." *Journal of Structural Engineering*. 114(7), pp. 1689-1699. 1988. https://doi.org/10.1061/(asce)0733-9445(1988)114:7(1689)

[10] Benedetti, A., Tralli A., "A New hybrid f.e. model for arbitrarily curved beam-I. Linear Analysis." *Computer Structures.* 33(6), pp, 1437-1449. 1989. https://doi.org/10.1016/0045-7949(89)90484-7

[11] Marquis, J. P., Wang, T. M. "Stiffness matrix of parabolic beam element." *Computer Structures*. 31(6), pp. 863–870. 1989. https://doi.org/10.1016/0045-7949(89)90271-x

[12] Lee, H. P. "Generalized stiffness matrix of a curved-beam element." *AIAA Journal*. 7(10), pp. 2043-2045. 1969. https://doi.org/10.2514/3.5513

[13] Gimena, L., Gonzaga, P., Gimena, F. N. "Finite Transfer Method, for the Problem of Spatially Curved Beams." In: Proceedings of the World Congress on Engineering, Vol. 2, WCE, London, July 2-4, 2008.

[14] Dahlberg, T. "Procedure to calculate deflections of curved beams." *International Journal of Engineering Education*. 20(3), pp. 503-513. 2004.

[15] Gendy, A. S., Saleeb, A. F. "On the finite element analysis of the spatial response of curved beams with arbitrary thin-walled sections." *Computers & Structures*. 44(3), pp. 639-652. 1992. https://doi.org/10.1016/0045-7949(92)90396-h

[16] Fam, A. R. M., Turkstra, C. "Model study of horizontally curved box girder." *Journal of the Structural Division, American Society of Civil Engineers.* 102, pp. 1097-1108, 1976.

[17] Yoo, C. H. "Matrix formulation of curved girders." *Journal of Engineering Mechanics Division, American Society of Civil Engineers*. 105, pp. 971-987. 1979.

[18] Bruno, A., Joslin, W., Moore, L. "The concepts of bias, precision and accuracy, and their use in testing the performance of species richness estimators, with a literature review of estimator performance." *Ecography*. 28(6), pp. 815-829. 2005. https://doi.org/10.1111/j.2005.0906-7590.04112.x